Characterization of a New Porous Pt-Containing Metal-Organic Framework Containing Potentially Catalytically Active Sites: Local Electronic Structure at the Metal Centers

Kai Chung Szeto,[†] Carmelo Prestipino,[‡,⊥] Carlo Lamberti,[‡] Adriano Zecchina,[‡] Silvia Bordiga,*[,‡] Morten Bjørgen,[†,§,∥] Mats Tilset,[†] and Karl Petter Lillerud*[,†]

Department of Chemistry, University of Oslo, P.O. Box 1033, N-0315 Oslo, Norway, Dipartimento di Chimica IFM and NIS Centre of Excellence, Università di Torino, via Pietro Giuria 7, I-10125 Torino, Italy, and INSTM Centro di Riferimento, Università di Torino, Torino, Italy, Haldor Topsøe A/S, Nymøllevej 55, DK-2800 Lyngby, Denmark, and Centre for Materials Science and Nanotechnology, University of Oslo, P.O. Box 1128, N- 0318 Oslo, Norway

Received July 15, 2006. Revised Manuscript Received October 7, 2006

A crystalline and thermally stable metal-organic framework (MOF) with Pt^{II} and Gd^{III} sites incorporated in the structure has been recently reported. This material has been synthesized with the aim to develop a heterogeneous Pt^{II} counterpart to homogeneous metal-organic complexes having C−H activating properties. The first account focused on the MOF synthesis and on structural and stability characterization of the material. In the present work, a multitechnique approach has been adopted to investigate the effect of solvent removal and the reversibility of this process. Structural features have been investigated by means of powder X-ray diffraction and extended X-ray absorption fine structure spectroscopy at both Pt and Gd L_3-edges. Electronic properties have been studied with diffuse reflectance surface UV−vis and X-ray absorption near-edge spectroscopies. Finally, IR spectroscopy has been used to determine the vibration properties. Thermogravimetric methods have been used to quantify the water loss. X-ray absorption spectroscopy has been used to compare the Pt environment in the periodic MOF structure, in related molecular complexes, and in the linkers. Our results demonstrate that the environment around Pt is more or less unaffected by the incorporation of the Pt centers in the molecular complexes into the 3D extended framework of the Pt−Gd MOF. The principle of using known homogeneous complexes as building blocks for the construction of single-site heterogeneous catalysts therefore seems applicable in the present case. Removal of solvent water molecules from the internal voids of the as-prepared MOF presents an opportunity to attain a porous material with accessible Pt^{II} sites. We observe that the structure undergoes a reversible loss of long-range order upon dehydration at ambient temperature. The environment of Gd is somewhat perturbed in the dehydration/hydration process, while that of Pt is almost unaffected. When a total dehydration is achieved, the original structure is only partially recovered upon rehydration.

1. Introduction

During the past decades, the direct, selective conversion of alkanes, methane in particular, into more valuable products has been subjected to extensive research efforts.[1−4] After the first example of direct homogeneous activation[5] and conversion[6] of methane by Pt under mild conditions was reported, a variety of homogeneous complexes that activate C−H bonds have been successfully developed.[4,7−9] These complexes are most often based on cis-coordinated N-donor organic ligands at a square planar Pt^{II} center. The reactivity toward alkane and arene C−H bonds is improved compared to the first examples, where the catalytic system operated in acidic aqueous solutions with dissolved K_2PtCl_4 as the catalyst. The utilization of such a catalytic system based on Pt^{II}−N donor ligand complexes has been described by Periana and co-workers who demonstrated a high-yield oxidation of methane to methyl bisulfate with dichloro(η^2-{2,2′-bipyrimidyl})Pt^{II} as the catalyst precursor in fuming H_2SO_4.[10]

Although quite robust organometallic complexes have been attained throughout the years, practical challenges including stability and recovery of the homogeneous catalyst have significantly impeded a commercialization of the process. Since heterogeneous systems are usually preferable in large-

* Corresponding authors: S. Bordiga: fax, +39 011 6707855; e-mail, silvia.bordiga@unito.it. K. P. Lillerud: fax, +47 2285 5441; e-mail, kpl@kjemi.uio.no.
† Department of Chemistry, University of Oslo.
‡ Università di Torino.
§ Haldor Topsøe A/S.
∥ Centre for Materials Science and Nanotechnology, University of Oslo.
⊥ Present address: ESRF, BP 220, F-38043 Grenoble, France.

(1) Shilov, A. E.; Shul'pin, G. B. *Chem. Rev.* **1997**, *97*, 2879−2932.
(2) Crabtree, R. H. *Chem. Rev.* **1995**, *95*, 987−1007.
(3) Labinger, J. A.; Bercaw, J. E. *Nature* **2002**, *417*, 507−514.
(4) Lersch, M.; Tilset, M. *Chem. Rev.* **2005**, *105*, 2471−2526.
(5) Gol'dshleger, N. F.; Tyabin, M. B.; Shilov, A. E.; Shteinman, A. A. *Russ. J. Phys. Chem.* **1969**, *43*, 1222−1223.
(6) Gol'dshleger, N. F.; Es'kova, V. V.; Shilov, A. E.; Shteinman, A. A. *Russ. J. Phys. Chem.* **1972**, *46*, 785−786.
(7) Holtcamp, M. W.; Labinger, J. A.; Bercaw, J. E. *J. Am. Chem. Soc.* **1997**, *119*, 848−849.
(8) Johansson, L.; Ryan, O. B.; Tilset, M. *J. Am. Chem. Soc.* **1999**, *121*, 1974−1975.
(9) Johansson, L.; Tilset, M.; Labinger, J. A.; Bercaw, J. E. *J. Am. Chem. Soc.* **2000**, *122*, 10846−10855.
(10) Periana, R. A.; Taube, D. J.; Gamble, S.; Taube, H.; Satoh, T.; Fujii, H. *Science* **1998**, *280*, 560−564.

10.1021/cm0616432 CCC: $37.00
Published on Web 12/21/2006

scale production, development of heterogeneous counterparts based on the well-known organometallic complexes might further promote the utilization of methane in a direct conversion process.

Very recently, we developed novel, thermally stable bimetallic metal-organic frameworks (MOFs) based on Pt^{II}, Gd,[11] or Y,[12] and 2,2′-bipyridine-5,5′-dicarboxylate (BPDC) with an extended framework structure. The Pt/Gd variant will hereafter be labeled as Pt/Gd-MOF.[11] According to the structure resulting from a single-crystal X-ray diffraction (XRD) analysis, coordination environment around Pt is quite similar to organometallic complexes that are able to activate and convert methane.[4,10] Fixing the active sites in a rigid lattice should preclude self-destruction, improve the thermal stability of a catalytic material, and facilitate efficient catalyst recovery. Our initial account of Gd[11] demonstrated a new principle for introducing active metal centers into MOF structure by using suitable bridge, creating MOF that is close mimics of already proven homogeneous C−H activating systems. It is of crucial importance to know how the electronic environment around the active metal center is altered by the incorporation into a 3D extended framework. This question is addressed here through a comparative study of the organometallic Pt complexes, the linkers, and the final MOF structure by the use of X-ray absorption spectroscopy.

For the potential catalytic use it is crucial to know how both the 3D network structure and the local environment around the metal centers respond to the removal of guest solvent molecules, which are water molecules in this case. The possibility of removing the guest water molecules represents an opportunity for achieving a permanent porous material with catalytically active sites exposed to the surroundings.

We present results describing how the 3D MOF structure and the local environment around the metal center respond to removal and reintroduction of solvent water. These changes are monitored by powder XRD, X-ray absorption fine structure spectroscopy (XAFS), transmission FTIR spectroscopy, diffuse reflectance surface UV−VIS (DRS UV−vis) spectroscopy, and thermogravimetric (TG) methods. A similar multi-technique characterization approach has been recently adopted to investigate the accessibility of Cu^{II} centers in HKUST-1 MOF.[13]

2. Experimental Section

The Pt/Gd-MOF was prepared according to the single-step procedure reported elsewhere.[11] The obtained material was dried in air at ambient temperature. Powder XRD was recorded with a Bruker AXS D5000 diffractometer equipped with Cu tube, Ge monocromator ($\lambda = 1.540598$ Å), and a BRAUN PSD (position-sensitive detector). The TG experiment was carried out with a Rheometric Scientific STA1500 instrument with a heating ramp of 10 °C/min. FTIR transmission spectra were collected at 2 cm^{-1} resolution with a Bruker IFS66 spectrophotometer equipped with a MCT detector. The sample was dispersed on a Si wafer by application of an aqueous slurry. Excess solvent was allowed to evaporate slowly at ambient temperature, leaving behind a thin layer of the sample on the Si wafer. The data collection was performed with a homemade quartz cell equipped with KBr windows, allowing thermal treatments and in situ studies of water desorption and re-adsorption. DRS UV−vis spectra were collected on a Perkin-Elmer λ19 spectrophotometer. The sample, in the form of a powder diluted with Teflon, was put in an optic quartz cell permanently attached to a vacuum line to allow in situ studies of water desorption and re-adsorption.

X-ray absorption experiments on Pt and Gd L_3-edges were performed at the BM29[14] beamline at the European Synchrotron Radiation Facility (ESRF). The monochromator was equipped with two Si(311) flat crystals and harmonic rejection was achieved using Rh-coated mirrors after the monochromator. The following experimental geometry was adopted: (1) I_0 (10% efficiency); (2) Pt/Gd-MOF sample; (3) I_1 (50% efficiency); (4) reference; (5) I_2 (80% efficiency).[15] This setup allows a direct energy/angle calibration for each spectrum, avoiding any problem related to slight energy shifts due to limited thermal instability of the monochromator crystals. For the XANES part a sampling step of 0.3 eV has been applied while for extended X-ray absorption fine structure spectroscopy (EXAFS) parts a constant sampling step in k-space ($\Delta k = 0.025$ Å^{-1}) has been used. For each sampled point an integration time of 3 s has been used. Spectra have been collected in the 6880−9000 eV and 11100−13710 eV ranges for Gd and Pt L_3-edges, respectively. Spectra have been collected at ambient temperature using a metallic cell, allowing in situ high-temperature treatments and gas dosage.[16] Due to the significant difference in energy between the Pt and Gd edges, the measurements have been performed in two different runs, allowing an optimization of the beamline (ionization chambers and mirror) and of the sample, as the ideal thickness is different for the two edges.

EXAFS analysis has been performed using Klementev's programs.[17] Phase and amplitudes have been calculated by FEFF 8.20 code[18] using as input the structure as solved by single-crystal X-ray diffraction.[11] Phase and amplitudes have been successfully checked with the model compounds $Gd(NO_3)_3 \cdot 6H_2O$ and $PtCl_2$.

The analysis of the EXAFS signals have been performed on back Fourier filtered signals. For the Pt L_3-edge we have adopted a k window from 3 to 16 Å^{-1}, with a k^3 weight, and R window of 1.3−2.60 Å: $2\Delta k \Delta R/\pi = 10.76$. For Gd L_3-edge, we have used a k window from 3 to 10 Å^{-1}, with a k^2 weight, and a R window of 1.3−2.90 Å: $2\Delta k \Delta R/\pi = 7.13$.

The charge at Pt has been evaluated on a series of Pt compounds, including the building block in the Pt/Gd-MOF. The method of charge assignment has been "Mulliken charges" as implemented by the Dmol^3 program packages from Accelrys Software, Inc. The basis set was DND, and the functionals were GGA, PW91; all electrons were treated relativistically. Molecular structures were

(11) Szeto, K. C.; Kongshaug, K. O.; Jakobsen, S.; Tilset, M.; Lillerud, K. P. *Dalton Trans*. Submitted.
(12) Szeto, K. C.; Lillerud, K.P.; Tilset, M.; Bjørgen, M.; Prestipino, C.; Zecchina, A.; Lamberti, C; Bordiga, S. *J. Phys. Chem. B* **2006**, *110*, 21509−21520.
(13) Prestipino, C.; Regli, L.; Vitillo, J. G.; Bonino, F.; Damin, A.; Lamberti, C.; Zecchina, A.; Solari, P. L.; Kongshaug, K. O.; Bordiga, S. *Chem. Mater*. **2006**, *18*, 1337−1346.
(14) Filipponi, A.; Borowski, M.; Bowron, D. T.; Ansell, S.; Di Cicco, A.; De Panfilis, S.; Itie, J. P. *Rev. Sci. Instrum*. **2000**, *71*, 2422−2432.
(15) Lamberti, C.; Bordiga, S.; Bonino, F.; Prestipino, C.; Berlier, G.; Capello, L.; D'Acapito, F.; Xamena, F. X. L. I.; Zecchina, A. *Phys. Chem. Chem. Phys*. **2003**, *5*, 4502−4509.
(16) Lamberti, C.; Prestipino, C.; Bordiga, S.; Berlier, G.; Spoto, G.; Zecchina, A.; Laloni, A.; La Manna, F.; D'Anca, F.; Felici, R.; D'Acapito, F.; Roy, P. *Nucl. Instrum. Methods B* **2003**, *200*, 196−201.
(17) Klementev, K. V. *Nucl. Instrum. Methods Phys. Res. A* **2000**, *448*, 299−301.
(18) Ankudinov, A. L.; Rave, L. B.; Rehr, J. J.; Conradson, S. D. *Phys. Rev. B* **1998**, *58*, 7565−7576.

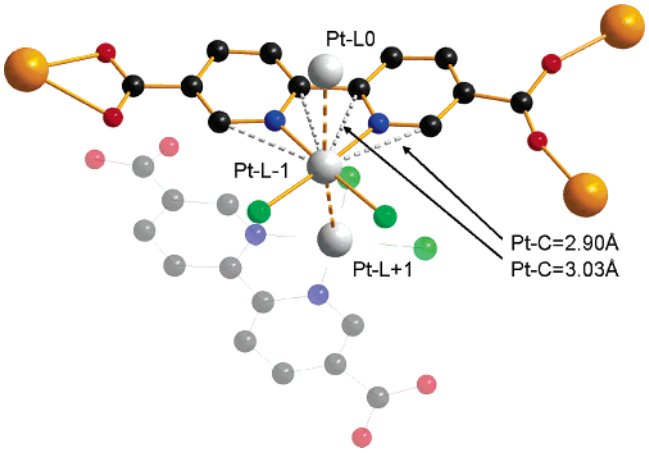

Figure 1. Local coordination around Pt based on single-crystal data. The Pt atom located in the layer below the focused layer is drawn with its coordinating atoms in faded colors, while the Pt atom above the focused layer is drawn for clarity only as a stripped Pt atom. Atom colors: Pt - gray, Gd - orange, Cl - green, N - blue, C − black, and O - red. The connotation of the Pt atoms as L0, L + 1, and L − 1 refer to the layer numbering used in Figure 4.

geometry-optimized, while the periodic calculations were based on the structure determined from X-ray diffraction.

3. Results and Discussion

3.1. Local Structure of Platinum and Gadolinium in Pt/Gd-MOF "as Made" Sample: XAFS Data.

3.1.1. Platinum Environment. The structure of the Pt/Gd-MOF, determined by single-crystal X-ray diffraction,[11] with focus on the local environment around Pt, is depicted in Figure 1 (see also Table S1 of the Supporting Information). The nonbonding but fairly close interactions between Pt and the C atoms neighboring to N in the pyridine rings are also included in the table. Figure 2a shows XANES spectra of the Pt L_3-edge. In particular, the Pt/Gd-MOF "as prepared" is compared with model compounds $PtCl_2$, K_2PtCl_4, and the complexes $(BPDC)PtCl_2$ (representing the organometallic building block), **A**, **B**, and **C**, whose structures are shown schematically in Scheme 1.

In the XANES spectra, the edge position reflects the electron density of the absorbing atom. As it is not a trivial task to correctly define the edge position, and as all the XANES spectra reported in Figure 2a exhibit an almost featureless shape characterized by a single maximum (white line), we arbitrarily use the white line position as a relative definition of the Pt L_3-edge position (the actual one occurring a few eV below).

The high sensitivity of the XANES edge position, reflecting the experimental electron density of Pt, is confirmed by the good correlation with the ab initio calculated electron densities at Pt in the series of molecular complexes investigated (Figure 2b).

The energy shift of the edge throughout the series is important and spans 2.3 eV from $PtCl_2$ to complex **C**. A much smaller range, 0.7 eV only, is observed among the four samples where Pt is coordinated by two Cl and two N atoms. In particular, the difference observed between the Pt/Gd-MOF and its molecular building block $(BPDC)PtCl_2$ is only 0.5 eV. As the similarities not only hold for the white

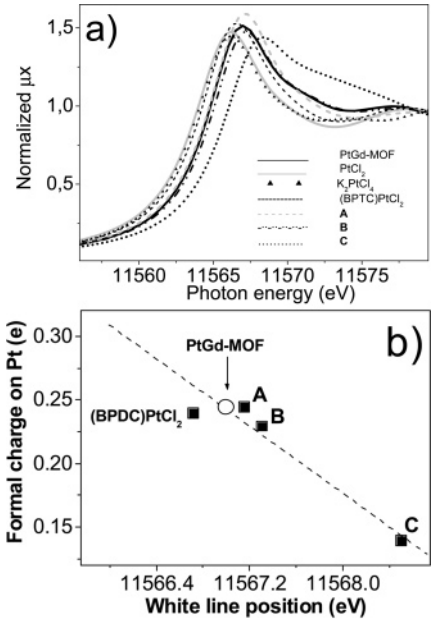

Figure 2. (a) Normalized Pt L_3-edge XANES spectra of Pt/Gd-MOF. Also included are $PtCl_2$, K_2PtCl_4, $(BPDC)PtCl_2$ (representing the organometallic building block), and the complexes **A**, **B**, and **C** as defined in Scheme 1. (b) Correlation between the ab initio calculated Mulliken charges at Pt (ordinate) and the white line position of the Pt L_3-edge XANES spectra reported in (a) (abscissa). Ab initio calculations have been performed on molecular compounds only.

Scheme 1

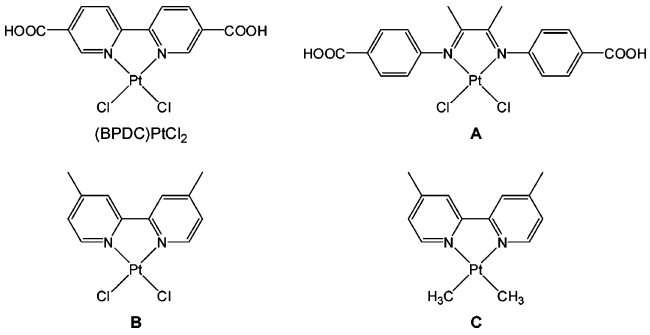

line position but also apply to the whole XANES region, we conclude that the local electronic structure around Pt in the Pt/Gd-MOF has not been significantly altered after incorporation of the complex into the extended framework.

Figure 3a reports the k^3-weighted EXAFS signal extracted from the "as-prepared" Pt/Gd-MOF material. Although it is mainly due to rather light scattering atoms (C, N, and Cl, see Figure 1), the EXAFS oscillations are clearly visible up to 18 $Å^{-1}$. This feature reflects an important homogeneity of the local environment of Pt in the material. Figure 3b reports the phase uncorrected, k^3-weighted FT of the EXAFS signal (dotted curves). The modulus (black dotted curve) exhibits two clear maxima centered around 1.6 and 2.0 Å due to N and Cl scattering, respectively.

The experimental curve has then been modeled as the sum of the contributions from the three closest atomic neighbors (see Figure 1 and Table 1): the two N atoms in the pyridine rings (Pt−N), the two Cl atoms directly bonded to Pt (Pt−Cl), and finally, the closest two C atoms in the pyridine rings (d(Pt−C) = 2.90(7) Å). The second pair of C atoms at the pyridine ring (d(Pt−C = 3.03(6) Å) and the close Pt−Pt

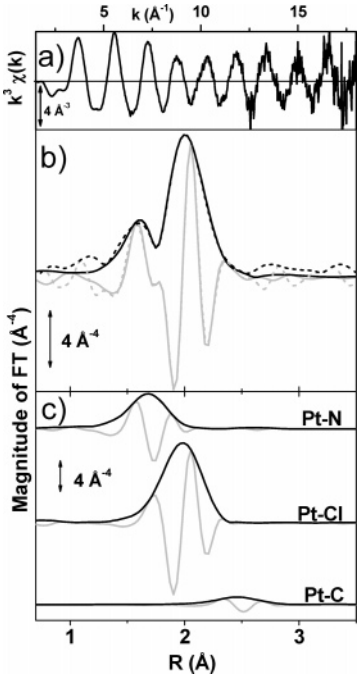

Figure 3. (a) k^3-weighted $\chi(k)$ function of the Pt/Gd-MOF. (b) Module (black) and imaginary (gray) parts for k^3-weighted FT of the Pt L_3-edge EXAFS function of the Pt/Gd-MOF shown in Figure 2a. Dotted and full lines refer to the experimental data and to the best fit, respectively. (c) Separate contributions of the N, Cl, and C atoms to the fitted EXAFS signal. Real and imaginary parts as in (b).

Table 1. Summary of the Optimized First-Shell Parameters Obtained from the EXAFS Data Analysis and the Single-Crystal XRD Data of Pt/Gd-MOF[a]

absorber/ scatterer	EXAFS				single-crystal XRD	
	R/Å	N	σ^2 10^{-3}/Å^2	ΔE/eV	<*R*>/Å	N
Pt−N	2.02(2)	1.9(2)	2.7(5)	5(1)	2.04(5)	2
Pt−Cl	2.303(8)	1.9	2.4(5)	5	2.309(17)	2
Pt−C[2]	2.86(4)	1.9	5.7(5)	5	2.88(7)	2
Gd−O	2.35(2)	8.6(10)	15(3)	1(1)	2.41(7)	8

[a] The EXAFS data analysis of the as-prepared Pt/Gd-MOF includes both the Pt L_3-edge (first three rows) and the Gd L_3-edge (last row). A comparison with the single-crystal XRD data[11] (last two columns) is included. In the Pt L_3 case the experimental signal has been optimized including a Pt−N, a Pt−Cl, and a Pt−C contribution. The reported values are averaged over the three crystallographically independent Pt sites (Figure 1, Figure 4, and Table S1 of the Supporting Information). The rather narrow distribution of distances in the three Pt sites (Table S1) results in a high-quality fit (Figure 3b). The experimental signal of the Gd L_3-edge was optimized using a unique Gd−O contribution. All corresponding parameters have consequently an average character. The large values of the optimized Debye−Waller factor reflects the heterogeneities of the Gd−O distances (in the 2.26−2.52 Å range, see Table S1) and has no dynamic significance. The parameters that have been fixed in the fit have no corresponding error bars.

distances (ca. 3.3 Å) have not been included in the signal. As the ranges of the direct- and back-FT fix the number of free parameters to $2\Delta R\Delta k/\pi = 10.7$, some constraints have to be applied. We decided to fit the three shells with the same coordination number N and the same energy shift ΔE_0. This results in a total number of eight fitted parameters: three distances, three Debye−Waller factors (σ), a single N, and a single ΔE_0. These constraints also have the advantage of reducing the correlation between the different variables. The quantitative results are listed in Table 1, while the quality of the fit can be evaluated in Figure 3b by comparing dotted and full line curves for both the moduli (black curves) and imaginary parts (gray curves). The individual contributions

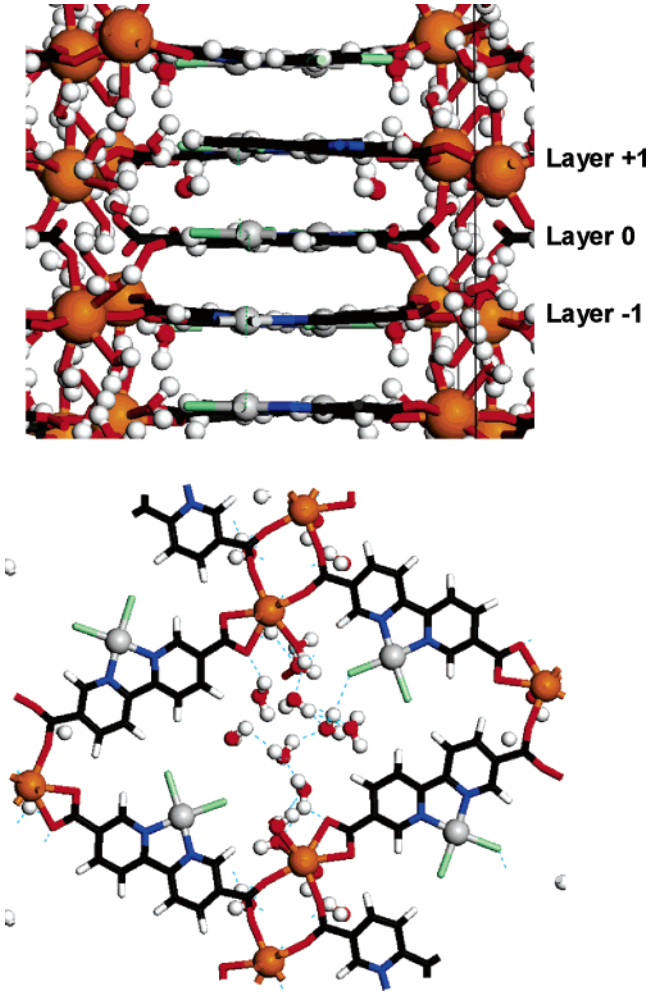

Figure 4. 3D representation of the Pt/Gd-MOF structure. The atoms of the (BPDC)$PtCl_2$ linker are reported using a sticks representation with C (black), N (blue), H (white), O (red), Cl (light green), and Pt (gray). The Gd atoms are depicted as enlarged orange spheres coordinated to the O atoms of the carboxylate groups with sticks. The water molecules are drawn with sticks and ball representation. Dashed lines represent H-bonding. Top: [100] view. The layers labeled as +1, 0, and −1 represent a block of layers connected along the [010] direction with covalent bonds. Adjacent blocks are not covalently bonded. Bottom: [010] view.

from the three modeled shells are reported separately in Figure 3c to appreciate the important relative differences. The quantitative results extracted form the EXAFS data analysis agree within the experimental errors with the corresponding values obtained by single-crystal XRD (Table 1).

3.1.2. Gadolinium Environment. The single-crystal diffraction data show four Gd atoms that connect the three layers of (BPDC)$PtCl_2$ linkers—two in the plane of the top layer (Layer +1) and two in the plane of the bottom layer (Layer −1). There are no Gd atoms in the plane of the middle layer of linkers (Layer 0); see Figure 4. The two crystallographically independent Gd atoms have similar coordination environments. The coordination sphere contains five oxygen atoms from four different (BPDC)$PtCl_2$ linker groups: one group in Layer 1 and −1 is attached to Gd via two oxygen atoms in a bidendate connection. The third oxygen is offered by a carboxylate located in Layer 0 (Figure 4), using only one oxygen to coordinate, thereby leaving the second oxygen atom uncoordinated. The two remaining oxygen atoms

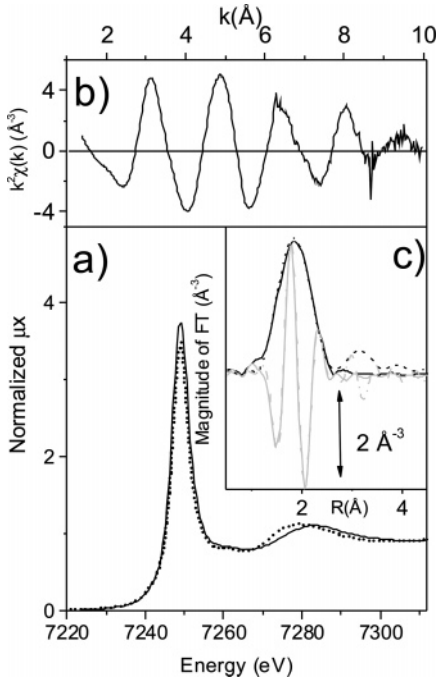

Figure 5. (a) Gd L_3 XANES region of Pt/Gd-MOF (full line) compared with the $Gd(NO_3)_3 \cdot 6H_2O$ reference compound (dotted line). (b) Gd L_3-edge, k^2 weighted, EXAFS signal extracted for Pt/Gd-MOF. (c) Corresponding k^2 weighted, phase uncorrected, FT (dotted lines) reported together with the best fit (full lines). Black and gray curves refer to the moduli and the imaginary parts, respectively.

originate from two independent carboxylate groups in Layer 1 and −1, where the carboxylates may be regarded to engage in a μ_2 linkage between two Gd atoms. Furthermore, three water molecules coordinate at each Gd. The Gd−O distances are distributed from 2.26 to 2.52 Å.

Figure 5a compares the Gd L_3 XANES region of Pt/Gd-MOF and the $Gd(NO_3)_3 \cdot 6H_2O$ reference compound. We note that the edge is dominated by a strong resonance at 7249.0 eV (white line) as high as 3.75 and 3.49 (normalized units) for Pt/Gd-MOF and $Gd(NO_3)_3 \cdot 6H_2O$, respectively. In the entire XANES region the spectra of the two materials are very similar.

This strong resonance has its origin in the transition between 2p core level and the completely empty 5d level; this energy is characteristic of the Gd^{3+} ion.[19] The characteristic weak shoulder at 7260 eV, a result of multiple scattering,[20] is practically absent in the spectra of the Pt/Gd-MOF. This underlines the broad distribution in Gd−O distances, as already inferred from the single-crystal data. The two curves are significantly different after the edge where, beside the similar amplitude in the EXAFS oscillation, a consistent difference in its period is observed. The last feature is consistent with the presence of shorter bond distances in the MOF material as far as Gd−O distances in the first coordination sphere are concerned.

The Gd L_3-edge, k^2-weighted EXAFS spectrum is reported in Figure 5b. In this case the useful signal extends up to 10 $Å^{-1}$ only, reflecting a much lower local order with respect to that present around Pt (see Figure 3). This is not unexpected, as XRD has shown a large spread in the first shell bond distances around Gd. The k^2-weighted FT is shown in Figure 5c for both modulus (black) and imaginary (gray) parts (dotted curves). In this case the EXAFS signal has been modeled only as an average of contribution from the first coordination shell arising from O atoms from both the carboxylate groups (five) and coordinated H_2O molecules (three). The corresponding best fit is reported as continuous curves in Figure 5c. The quantitative results are reported in Table 1. It is important to recall that the result from single-crystal diffraction led to a single-shell model of Gd with eight oxygen atoms around Gd, but with broad distribution of distances between 2.26 and 2.52 Å (see Table S1 of the Supporting Information). This broad distribution results in an unusually high Debye−Waller factor: $\sigma^2 = 0.015$ Å^2, which is mainly of static rather than dynamic nature. As a consequence, the optimized first-shell Gd−O distance ($R = 2.35 \pm 0.02$ Å) has just an average meaning and appears compressed with respect to the average distance calculated from the XRD structure (Table 1). This apparent disagreement results from the well-known underestimation of bond lengths that occurs when the classical EXAFS data analysis is adopted on samples characterized by a large structural disorder of bond lengths. The effect of a large disorder is equivalent to that of a system having an asymmetrical radial distribution function, which can lead to an apparent contraction of bond lengths in the usual analysis of EXAFS data.[21−25]

3.1.3. Summary of the Structural Investigation. XRD and XAFS are complementary techniques. XRD reveals the periodic average from the crystalline material while the XAFS gives information about the local environment around the investigated metal centers with some additional information on their electronic structure. The results demonstrate that the environment around Pt is quite unaffected by incorporation of the Pt center of the molecular complexes into the 3D Pt/Gd-MOF. Thus, the principle of using well-established molecular systems as models for the construction of heterogeneous single-site catalysts appears to be applicable. The comparison of XRD and XAFS structural data for the Pt/Gd-MOF, summarized in Table 1, shows excellent agreement as the differences in the reported values lie within the uncertainties in measurements. Despite the technical reasons outlined above, the differences in Gd−O distances are also within the experimental uncertainties.

3.2. Location of Water, Dehydration, and Rehydration Process. Figure 6 illustrates the free volume accessible to solvent water in Pt/Gd-MOF material. The surface is created as a Connolly surface (1.4 Å radius to model the solvent) after removing water from the structure model. This volume

(19) Wu, Z. Y.; Benfatto, M. *J. Phys. IV* **1997**, *7*, 167−168.
(20) Wu, Z. Y.; Benfatto, M.; Natoli, C. R. *Phys. Rev. B* **1998**, *57*, 10336−10339.
(21) De Crescenzi, M.; Balzarotti, A.; Omin, F.; Incoccia, L.; Mobilio, S.; Motta, N. *Solid State Commun.* **1981**, *37*, 921−923.
(22) Marques, E. C.; Sandstrom, D. R.; Lytle, F. W.; Greegor, R. B. J. *Chem. Phys.* **1982**, *77*, 1027−1034.
(23) Lamberti, C.; Bordiga, S.; Zecchina, A.; Salvalaggio, M.; Geobaldo, F.; Otero, Areán, C. *J. Chem. Soc., Faraday Trans.* **1998**, *94*, 1519−1525.
(24) Lamberti, C.; Turnes Palomino, G.; Bordiga, S.; Zecchina, A.; Spano, G.; Otero Areán, C. *Catal. Lett.* **1999**, *63*, 213−216.
(25) (a) Berlier, G.; Spoto, G.; Fisicaro, P.; Bordiga, S.; Zecchina, A.; Giamello, E.; Lamberti, C. *Microchem. J.* **2002**, *71*, 101−116. (b) Bus, E.; Miller, J. T.; Jeremy Kropf, A.; Prins, R.; van Bokhoven, J. A. *Phys. Chem. Chem. Phys.* **2006**, *8* 3248−3258.

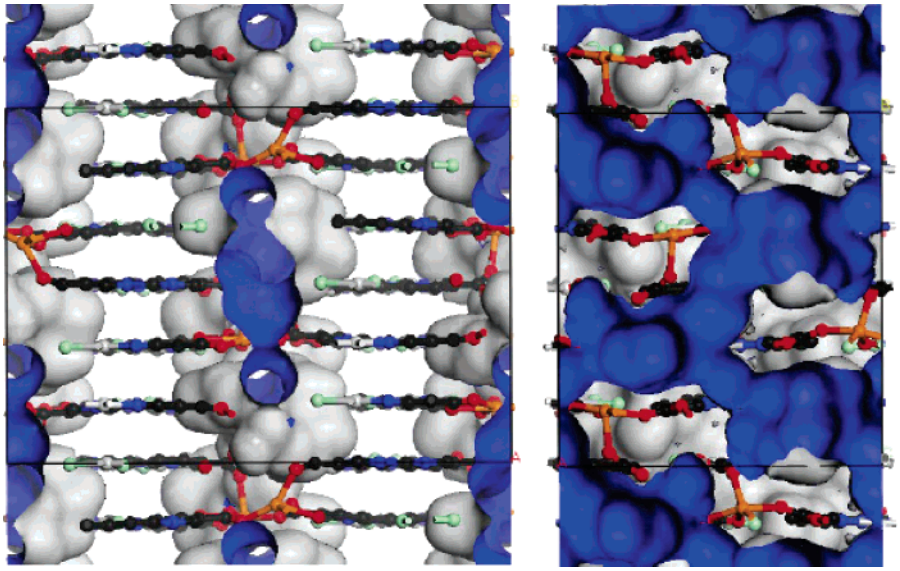

Figure 6. Illustration of the volume accessible to water in the Pt/Gd-MOF material. Connolly surface (blue internal and gray external) is created with a spherical probe with 1.4 Å radius. The left picture shows a projection along the [100] direction, while the right picture shows a view orthogonal to the 2D channel system, along the [001] direction. The MOF framework is represented as ball and sticks with the same color code as in Figure 4.

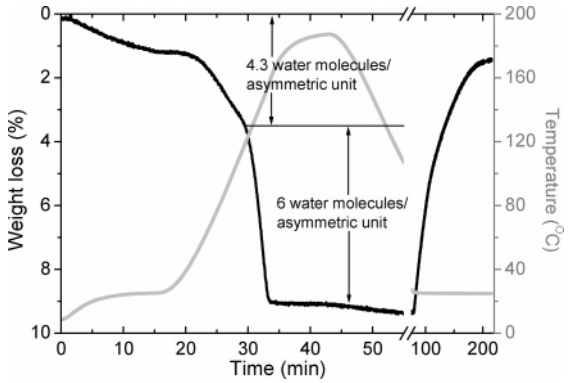

Figure 7. TG curve of the as-synthesized Pt/Gd-MOF showing the water removal obtained with a heating ramp of 10 °C/min and the following water uptake. The relative weight loss is reported vs time as full line (left ordinate), while the evolution of the sample temperature (dotted curve) refers to the right ordinate axis.

creates a connected 2-D channel structure around the (002) plane formed by the Gd atoms.

From single-crystal diffraction data[11] it has been evidenced that, in addition to the three water molecules coordinated to Gd, there are 5.5 water molecules in the asymmetric unit. Most of this free water is located in the quite large volume between the Gd dimers that are separated by about 13 Å in the [100] direction (see Figure 4b). This water is involved in an extensive hydrogen-bonding network (broken lines in Figure 4b) that also involves the carboxylate oxygen atoms and the water molecules coordinated to Gd.

3.2.1. Thermogravimetric Measurements. Water removal from the Pt/Gd-MOF was followed by thermogravimetric (TG) measurements. It is found that water leaves the structure in two steps (Figure 7), the first one from ambient temperature to 100 °C and the second one from 100 to 120 °C. The latter is followed by a stability plateau up to 350 °C, as demonstrated by monitoring the evolution of the XRPD pattern as a function of the temperature.[11]

The first step in the water loss process involves the free water molecules. It is worth noticing that some weight loss starts already in the dry N_2 atmosphere before the heating is started. This fact, accompanied by the slight slope of the curve, indicates that the system loses the free water very easily. On a quantitative ground this weight loss, measured as equivalent to 4.3 water molecules per asymmetric unit, is slightly lower than the 5.5 molecules found as free water in the single-crystal refinement.[11] The second weight loss step occurs from 100 to 120 °C and is sharp and corresponds exactly to six water molecules per asymmetric unit. This is equivalent to the number of water molecules coordinated to the Gd atoms present in the asymmetric unit.[11]

After drying the Pt/Gd-MOF at 180 °C, and subsequently exposing it to a carrier gas saturated with water (Figure 7, right part), the material regains the original water content (98.6 wt %).

3.2.2. X-ray Diffraction: A Qualitative Investigation Supported by Molecular Mechanics. An attempt was made to investigate the structure of the dehydrated Pt/Gd-MOF sample by single-crystal X-ray diffraction collected at 120 °C at the ID11 beamline of the ESRF storage ring. The high-temperature single-crystal measurement of the Pt/Gd-MOF revealed that removal of water introduces stress that destroys the single crystal. After water removal, the frames observed in the CCD area detector were similar to what is observed for highly textured powder patterns. Consequently, the single-crystal data will not be further discussed.

The structural change upon water removal was followed by powder XRD (XRPD) techniques instead. The Pt/Gd-MOF was hosted inside a capillary that was evacuated and sealed. The effect of dehydration and rehydration is reported in Figure 8: hydrated sample (a), sample dehydrated at room temperature (b), and rehydrated sample obtained upon capillary exposure to atmosphere (c).

The as-synthesized material (Figure 8a) is characterized by a high crystallinity, showing well-defined reflections up to $2\theta > 70°$. It is known that MOF materials that are organized in sheets can undergo crystallographic changes after removal of the solvent, resulting in different XRPD

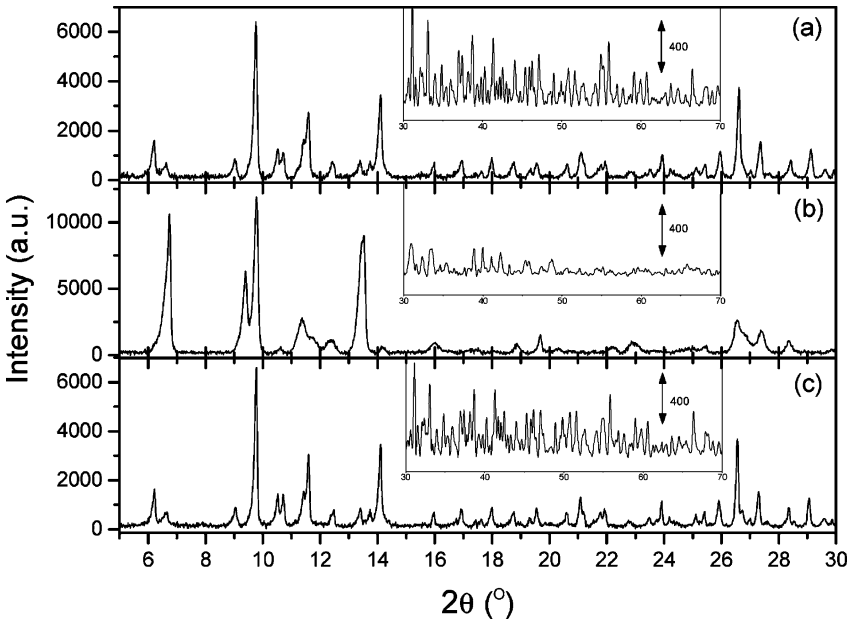

Figure 8. XRPD patterns of (a) as-prepared Pt/Gd-MOF material, (b) the dehydrated phase obtained by evacuation at ambient temperature (the sample was maintained in dehydrated form by sealing the capillary), and (c) after exposure of the previously evacuated sample to air. Data in the high 2θ insets have been smoothed with a 10 pt FFT routine.

Table 2. Evolution of the Unit Cell Parameters of the Pt/Gd-MOF upon Different Dehydration and Re-hydration Conditions[a]

cell parameters	as-synthesized	dehydrated at ambient T	dehydrated at 120 °C	rehydrated
a (Å)	18.13	18.50	18.79	18.06
b (Å)	19.99	19.53	19.73	20.00
c (Å)	28.35	27.06	26.97	28.37
V (Å^3)	10275	9777	9996	10247

[a] Values obtained from XRPD data.

patterns while the chemical building blocks are maintained.[13,26] Accordingly, water removal from the Pt/Gd-MOF (Figure 8b) causes dramatic changes in the XRPD pattern, where the peaks have undergone significant broadening. Notwithstanding this significant modification of the XRPD pattern after water removal at ambient temperature, the dehydration process is reversible as the subsequent exposure to the atmosphere restores the original XRPD pattern; compare parts (c) and (a) of Figure 8.

A structural refinement of the dehydrated phase has been attempted, but a combination of probable presence of preferred orientation, limited quality of the diffraction data, and the complexity of the structure prevents a full refinement with the powder data. The powder patterns for the dehydrated material have been indexed and then refined by using the whole profile in a Pawley refinement (the result of this refinement is shown in Figure S1 of the Supporting Information). Unit cell parameters for as-synthesized, dehydrated, and rehydrated materials are listed in Table 2.

Water removal causes a substantial reduction in the *c*-axis length, a small decrease of the *b*-axis, and a small increase of the *a*-axis (Table 2). The small shortening of *b*-axis, which is orthogonal to the layers formed by the (BPDC)$PtCl_2$ linkers, indicates a small reduction in the interlayer voids (Figure 4, top). In fact, in the hydrated material the layer separations are about 3.3 Å. Now, as the *b*-axis length in the ambient-temperature dehydrated material corresponds to an average layer separation of 3.26 Å, a value which is very close to the Pt−Pt distance in Layers 0 and −1 (3.29 Å), we conclude that upon dehydration the porosity of the material is not compromised. The most relevant change occurs in the *c*-axis relaxation and is due to a rearrangement. This interpretation is compatible with the reversible nature of the dehydration/hydration process probed by the XRPD experiment that is reported in Figure 8.

The lack of a full refinement of the anhydrous material forced us to find an alternative approach to model the structure of this phase. The refined structure of the hydrated phase was used as the starting point, all the water molecules were removed, and a structure optimization was performed by molecular mechanics (MM). In this process, the cell parameters were taken to be those obtained by XRPD on the anhydrous material (120 °C dehydration, see Table 2), and the (BPDC)$PtCl_2$ linkers were considered as rigid objects.

The results of the MM optimization is reported in Figure 9, [010] view. A comparison with the analogous view of the as-synthesized Pt/Gd-MOF (Figure 4, bottom) suggests that the main features of the structure are largely preserved in the dehydration process.

There is considerable flexibility around the Gd atoms that allows the structure to adapt reasonable bond lengths and angles in the new, slightly smaller cell. A qualitative evaluation of the diffraction patterns may indicate a substantial structural change. Reflections with (*h*00) indices are strongly enhanced: this is particularly noticeable for the (200) peak. This could be explained by an alignment of the Gd positions. A look at the changes in unit cell parameters and how the (BPDC)$PtCl_2$ linkers easily might be arranged to fit both cells reveals that the structural changes are minor and that the process might be fully reversible. The most significant changes occur in the vicinity of the Gd atoms.

(26) Edgar, M.; Mitchell, R.; Slawin, A. M. Z.; Lightfoot, P.; Wright, P. A. *Chem. Eur. J.* **2001**, *7*, 5168−5175.

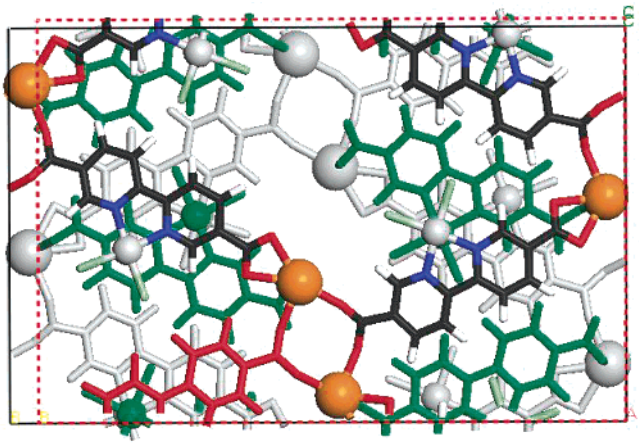

Figure 9. Model of the anhydrous Pt/Gd-MOF material, as obtained from MM optimization, [010] view. The original cell from the as-prepared material is included for comparison (full line).

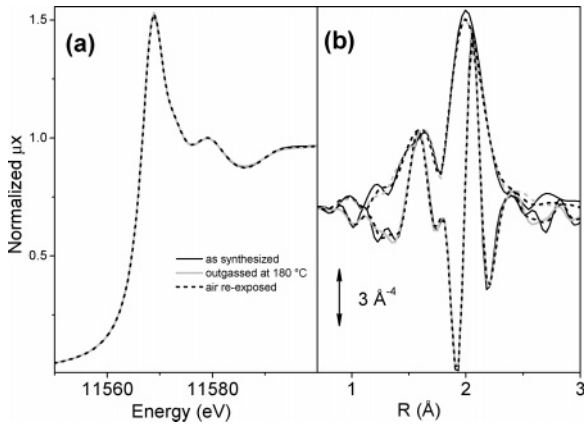

Figure 10. (a) Pt L_3-edge XANES spectra of Pt/Gd-MOF: as-synthesized (full black curve); dehydrated at 180 °C (full gray curve); re-exposed to air (black dotted curve). (b) k^3-weighted FT of the corresponding EXAFS spectra, line code as in (a). Both moduli and imaginary parts are reported.

3.2.3. X-ray Absorption of Dried Material. The absence of a full refinement of the powder XRD pattern of the anhydrous material makes XAFS a particularly attractive alternative in this case. EXAFS spectra at both Pt and Gd edges were collected also after sample outgassing at 180 °C, i.e., in the middle of the stability plateau observed in the TG experiment (Figure 7). The dehydration at ambient temperature has not been considered since the removal of the free water molecules is not supposed to affect the local environments of the Pt or Gd atoms.

Figure 10a reports the Pt L_3 XANES edges of the as-synthesized Pt/Gd-MOF (full black curve) of the sample after outgassing at 180 °C (full gray curve) and after subsequent re-exposure to air (dotted black curve). The three spectra are virtually indistinguishable. The same holds for the k^3-weighted FT of the corresponding EXAFS spectra, reported in Figure 10b with the same line code as in part (a). From the X-ray absorption data, we conclude that both the electron density and the first coordination sphere at Pt remain practically unchanged upon water evacuation. These findings confirm the notion that water molecules never penetrate the primary coordination sphere of Pt and that the (BPDC)$PtCl_2$ units remain stable during the dehydration/rehydration treatment.

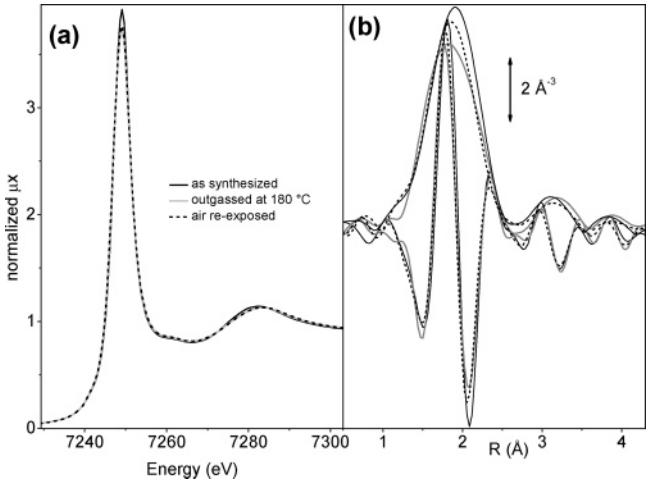

Figure 11. (a) Gd L_3-edge XANES spectra of Pt/Gd-MOF: as-synthesized (full black curve); dehydrated at 180 °C (full gray curve); re-exposed to air (black dotted curve). (b) k^2-weighted FT of the corresponding EXAFS spectra with same line code as in (a). Both moduli and imaginary parts are reported.

A different picture emerges from the X-ray absorption data collected at the Gd L_3-edge (Figure 11). In the XANES spectra (Figure 11a) the strong resonance at 7249.0 eV (white line) is slightly eroded by degassing and it is not completely restored upon exposure to air. A small change in the period of the first oscillation is also detected. A much more important effect is observed in the FT of EXAFS spectra; see Figure 11b. The dehydration procedure strongly affects the intensity and position of the peak that is due to the Gd−O contributions; this peak moves from 1.91 to 1.83 Å (phase uncorrected values) and decreases in intensity. This shortening of the average Gd−O distance by about 0.1 Å is a typical effect of ligand removal[13,27−31] and is not completely reversible as the subsequent exposure to ambient atmosphere only partially restores the initial spectrum. The Gd EXAFS signal is affected by water removal, clearly showing a decrease in the number of coordinated oxygen atoms. This change in coordination is accompanied by a small rearrangement in the local structure with a slight decrease in Gd−O distances and rearrangements outside the primary coordination sphere, ascribed to the presence of carboxyl groups of the (BPDC)-$PtCl_2$ units. This picture confirms that Gd is the more flexible species of the framework and that the long-order variation detected by diffraction is principally due to variation of the local order around Gd.

3.2.4. FTIR Spectroscopy. Spectrum 1 in Figure 12 presents vibrational properties of the as-synthesized sample while spectra 2−4 were collected at increasing times of outgassing (from 10 s to 20 min) at ambient temperature. The complete disappearance of the water modes is observed upon a vacuum thermal treatment at 180 °C (curve 5). When

(27) Zecchina, A.; Bordiga, S.; Palomino, G. T.; Scarano, D.; Lamberti, C.; Salvalaggio, M. *J. Phys. Chem. B* **1999**, *103*, 3833−3844.
(28) Lamberti, C.; Palomino, G. T.; Bordiga, S.; Berlier, G.; D'Acapito, F.; Zecchina, A. *Angew. Chem., Int. Ed.* **2000**, *39*, 3833−3844.
(29) Palomino, G. T.; Bordiga, S.; Zecchina, A.; Marra, G. L.; Lamberti, C. *J. Phys. Chem. B* **2000**, *104*, 8641−8651.
(30) Bordiga, S.; Damin, A.; Bonino, F.; Zecchina, A.; Spanò, G.; Rivetti, F.; Bolis, V.; Lamberti, C. *J. Phys. Chem. B* **2002**, *106*, 9892−9905.
(31) Prestipino, C.; Capello, L.; D'Acapito, F.; Lamberti, C. *Phys. Chem. Chem. Phys.* **2005**, *7*, 1743−1746.

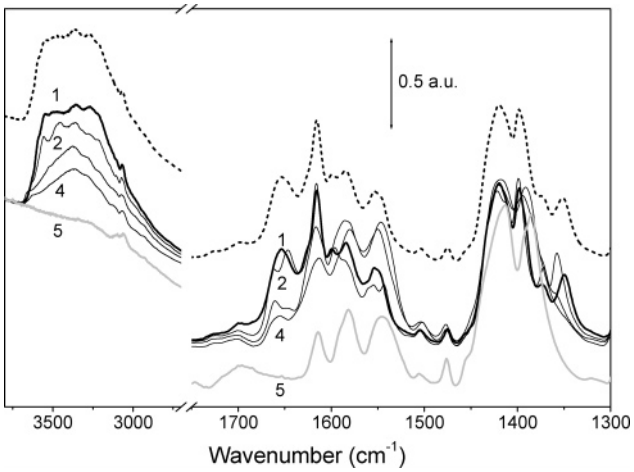

Figure 12. Effect of dehydration on the vibrational properties of Pt/Gd-MOF sample followed by in situ FTIR spectroscopy. Curve 1, as-synthesized material; curves 2−4, increasing time of outgassing at RT (10 s, 1 min, 20 min). Curve 5 shows the effect of outgassing at 180 °C. Dotted curve reports the effect of re-hydration upon H_2O dosage from the gas phase. Left and right parts refer to the OH-stretching and framework modes, respectively.

spectrum 4 had been collected, water vapor was dosed to the IR cell and resulted in the spectrum represented by the upper dotted curve.

Spectrum 1 (as-synthesized sample) shows a broad and unresolved band extending from 3680 to 2800 cm^{-1} (left part), mainly originating from ν(OH) modes of water confined in the pore system. The corresponding δ(OH) water bending mode gives the absorption at 1652 cm^{-1} (right part). Water molecules located within the nanopores of the solid are clearly engaged in medium-strength hydrogen bonds since the O−H stretching and bending modes are red-shifted and blue-shifted, respectively, with respect to the modes of the free molecule. The low-frequency region of the spectrum is characterized by a multiplet of combination modes of carboxylate species mixed with bands from bipyridine ring deformations.[32−35] Bipyridine units are characterized by an intense component at about 1590 cm^{-1} and a doublet at about 1460 and 1370 cm^{-1}. The carboxylate groups should give rather intense doublets in the ranges 1630−1500 and 1460−1350 cm^{-1} for asymmetric and symmetric stretching modes, respectively. The observed spectrum is much more complex, showing two groups of at least four components in the range 1620−1500 and 1420−1350 cm^{-1}, a region where it is difficult to differentiate the contributions of the carboxylate species from those of the bipyridine groups.

Water desorption at ambient temperature (spectra 2−4) leads to rather evident changes in the vibrational properties of the system. The intensities of the water stretching and bending modes are gradually reduced but do not completely disappear upon ambient temperature desorption. The composite band at 1652 cm^{-1}, assigned to water bending, separates into two components at 1661 and 1646 cm^{-1} (spectrum 2). The band at 1646 cm^{-1} is rapidly eroded, whereas the component at 1661 cm^{-1} is rather persistent and undergoes a small blue shift. This behavior is in perfect agreement with the presence of two families of water molecules as previously described. We can easily assign the component at 1661 cm^{-1} to water directly coordinated to Gd (strongly perturbed and more persistent) and the band at 1646 cm^{-1} to nearly free water molecules.[36−38]

The fact that the band at 1661 cm^{-1} undergoes a small blue shift can be explained by considering that this water is directly bonded to Gd. Upon thermal treatment at 180 °C (curve 5), a total erosion of H_2O components is observed, testifying to the complete dehydration of the sample.

In the region associated with the framework modes, both the positions and the intensity ratios of the maxima change. The most pronounced changes can be summarized as follows: The component at 1614 cm^{-1} progressively decreases in intensity, the doublets at 1598 and 1584 cm^{-1} give rise to a component at 1580 cm^{-1}, the band at 1552 cm^{-1} increases in intensity and shifts at 1547 cm^{-1}, and the four components at lower frequency (1418, 1399, 1371, and 1350 cm^{-1}) give rise to a doublet with maxima at 1417 and 1390 cm^{-1}.

The FTIR observations essentially confirm that water was indeed confined to the internal voids and thus interacted with the framework. When water was re-admitted to the cell, the vibrational properties of the material that was evacuated at ambient temperature were fully regained as shown by the upper dotted curve in Figure 12.

XRPD and Gd L_3-edge XAFS data have shown that, upon rehydration of a sample treated at high temperature, the long-range order is not totally recovered due to variation of the local order around Gd. The total reversibility of the IR features are only observed on a sample outgassed at room temperature. However, the local environment of Gd barely affects the vibrational modes of the material in the mid-IR region. We imagine that far-IR data, where the ν(Gd−O) modes are expected to appear, would have shown a partial reversibility on a sample treated at high temperature, in agreement with what is found by XRPD and XAFS.

3.2.5. Diffuse Reflectance Surface UV−Vis Spectroscopy. Removal of water from the as-synthesized material induces a color change from bright red to dark brown/red, indicating that water affects the electronic transitions of the system. Figure 13 displays the DRS UV−vis spectra of the as-synthesized sample (black solid curve), of the dehydrated phase obtained by evacuation at ambient temperature (gray solid curve), and after reintroduction of water (black dotted curve). No further significant changes are observed upon dehydration at 180 °C. The edge in the visible region, around 19000 cm^{-1} for the as-synthesized sample, is associated with Cl to Pt charge transfer. The strong intensity of this edge prevents the observation of the weaker features arising from

(32) Neto, N.; Muniz-Miranda, M.; Agneloni, L.; Castellucci, E. *Spectrochim. Acta* **1983**, *39A*, 97−106.
(33) Muniz-Miranda, M.; Castellucci, E.; Neto, N.; Sbrana, G. *Spectrochim. Acta* **1983**, *39A*, 107−113.
(34) Mordzinski, A.; Kownacki, K.; Les, A.; Oyler, N. A.; Adamowicz, L.; Langkilde, F. W.; Wilbrandt, R. *J. Phys. Chem.* **1994**, *98*, 5212−5220.
(35) Wang, F.; Berglund, K. A. *Ind. Eng. Chem. Res.* **2000**, *39*, 2101−2104.
(36) Al-Abadleh, H. A.; Grassian, V. H. *Langmuir* **2003**, *19*, 341−347.
(37) Beta, I. A.; Böhlig, H.; Hunger, B. *Phys. Chem. Chem. Phys.* **2004**, *6*, 1975−1981.
(38) Bordiga, S.; Regli, L.; Lamberti, C.; Zecchina, A.; Bjørgen, M.; Lillerud, K. P. *J. Phys. Chem. B* **2005**, *109*, 7724−7732.

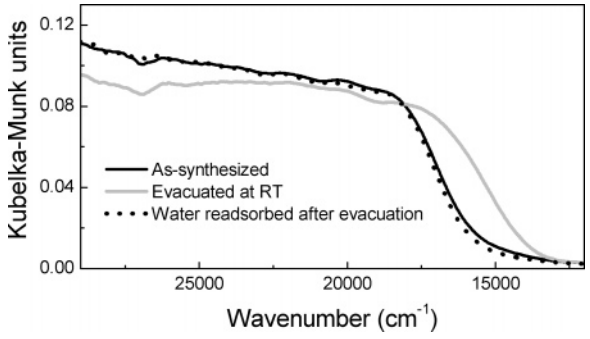

Figure 13. DR−UV/vis spectra of the as-synthesized Pt/Gd-MOF sample (black, solid curve), dehydrated phase obtained by evacuation at ambient temperature (solid gray curve), and after reintroduction of water (black dotted curve).

electronic transitions involving Gd corner stones and the organic linker, which are expected above 30000 cm^{-1}.[39]

The edge at 19000 cm^{-1} is downward shifted by about 2000 cm^{-1} when water is removed, but moves back to its original position when water is reintroduced into the system. This result means that even though there is no evidence of water directly associated to Pt or to Cl, water removal does interfere with the electronic properties of the Pt species and its first shell ligands. We hypothesize that, upon water elimination, the electron density increases around the chlorine atoms, with a resultant red shift for the ligand-to-metal charge-transfer transition. This observation suggests that these materials cannot be completely described in terms of the properties of their single building blocks only (these details were not discernible by XAFS analysis). This effect may originate in the fact that since the organic ligand is a full π-conjugated system, a change in coordination sphere of Gd (water removal) perturbs the carboxyl groups which are part of the linker and so modifies the charge density at Pt, as evidenced by the substantial change in the UV−vis spectrum of the partially dehydrated sample (Figure 13). This charge rearrangement upon water removal, which significantly affects the valence band of the material (Figure 13), has essentially not perturbed the Pt core levels, as testified by the virtual invariance of the Pt L_3-edge XANES spectra (Figure 10a). (Note that the two spectroscopic methods operate in photon energy domains that are separated by 3 orders of magnitude since 1 eV corresponds to almost 8000 cm^{-1}.)

(39) Collison, D.; Mabbs, F. E.; McInnes, E. J. L.; Taylor, K. J.; Welch, A. J.; Yellowless, L. J. *J. Chem. Soc., Dalton Trans.* **1996**, 329−334.

4. Conclusion

It has been demonstrated that a room-temperature dehydration process is able to remove almost all water molecules hosted inside the pores of the 3D Pt/Gd-MOF framework and that this process is fully reversible. Hence, at room temperature, a permanent porous material with potentially active sites can be obtained. Although the room-temperature dehydrated material shows a partial loss in the long-range order, the crystallinity is fully restored by rehydration, confirming that this material is not air- or moisture-sensitive. The reversibility is partially lost when the water removal becomes complete by dehydration above 120 °C.

X-ray absorption spectroscopy allows comparison of the metal environment in the molecular precursors and suitable models, linkers, and the periodic MOF structure. Our results demonstrate that the environment around Pt is more or less unaffected by the incorporation of the Pt centers in the complexes into the 3D Pt/Gd-MOF. The principle of using known homogeneous catalysts as models for the construction of single-site heterogeneous catalysts therefore seems to be applicable.

Acknowledgment. K.C.S. and M.B. are grateful for financial support from the Norwegian Research Council through Grant 158552/441 and Marie Curie Fellowship Association. S.B, A.Z., and C.L. are grateful for financial support from the INSTM progetto PRISMA and Compagnia di San Paolo. European Synchrotron Radiation Facility (ESRF) is also acknowledged for the invitations to experiment number CH-1700 and CH-1919. The important and friendly support by P. L. Solari during XAFS experiment at BM29 (CH-1700) is gratefully acknowledged. The same holds for the ID11 staff during single-crystal data collection. Søren Jakobsen, Martin Lersch, and Irene Fjeldahl Johannesen are kindly acknowledged for preparing the compounds (BPDC)$PtCl_2$, **A**, **B**, and **C**.

Supporting Information Available: Additional experimental section including text, tables, and figures. This material is available free of charge via the Internet at http://pubs.acs.org.

CM0616432